Design and Analysis of a Stiffened Composite Structure Repair Concept

Adam Przekop[1]
Analytical Services and Materials, Inc., Hampton, VA, 23666

A design and analysis of a repair concept applicable to a stiffened thin-skin composite panel based on the Pultruded Rod Stitched Efficient Unitized Structure is presented. Since the repair concept is a bolted repair using metal components, it can easily be applied in the operational environment. Initial analyses are aimed at validating the finite element modeling approach by comparing with available test data. Once confidence in the analysis approach is established several repair configurations are explored and the most efficient one presented. Repairs involving damage to the top of the stiffener alone are considered in addition to repairs involving a damaged stiffener, flange and underlying skin. High fidelity finite element modeling techniques such as mesh-independent definition of compliant fasteners, elastic-plastic metallic material properties and geometrically nonlinear analysis are utilized in the effort. The results of the analysis are presented and factors influencing the design are assessed and discussed.

Nomenclature

A	=	fastener's cross-section area
α_s	=	shear correction factor of 4/3
d	=	fastener's diameter
E	=	Young's modulus
ε	=	strain
G	=	shear modulus
H	=	plastic modulus
I	=	area moment of inertia
J	=	polar moment of inertia
K	=	fastener's stiffness
L	=	fastener's length
P	=	force
t	=	thickness
v	=	Poisson's ratio
S	=	stiffness around fastener cut-out
σ	=	stress
t	=	thickness
X, Y, Z	=	global coordinates

Subscripts

B	=	bearing
BP	=	bypass
R	=	rotational
s	=	shell
T	=	translational
$1, 2, 3$	=	local coordinates

[1] Senior Structural Engineer, c/o NASA Langley Research Center, Hampton, VA 23681, Mail Stop 463, Senior Member AIAA.

I. Introduction

The structural concept being pursued as an important component of next generation airframe technology under the Environmentally Responsible Aviation Program at NASA[1-6] is the Pultruded Rod Stitched Efficient Unitized Structure (PRSEUS), illustrated in Figure 1. This concept is being developed in a partnership between NASA and The Boeing Company for application to future transport aircraft with the goal of developing lighter structure so that the aircraft will require less fuel and produce fewer pollutants. The PRSEUS structure is highly-integrated, weight-efficient and has crack-arresting capabilities. In this concept a stitched carbon-epoxy material system is used. By stitching through the thickness of a dry carbon-epoxy material system, the labor associated with panel fabrication and assembly can be significantly reduced. When stitching through the thickness of pre-stacked skin, stringers, and frames, the need for mechanical fasteners is almost eliminated. In addition, stitching reduces delamination and improves damage tolerance, allowing for a lighter structure with more gradual failures than traditional composites without through-the-thickness reinforcement. The PRSEUS concept consists of carbon-epoxy panels fabricated from dry components and then infused in an oven while subjected to vacuum pressure. Skins, flanges and webs are composed of layers of carbon material forms that are pre-kitted in multi-ply stacks. A single stack contains seven plies (+45, -45, 0, 90, 0, -45, +45) where the 0-degree plies are approximately twice the thickness of the $\pm$45- and 90-degree plies, resulting in a 0.052 in. stack thickness with percentage of the 0°, 45° and 90° fibers equal to 44.9, 42.9 and 12.2, respectively. Several stacks of the pre-kitted material are used to build up the desired thickness and configuration. Stiffener flanges are stitched to the skin and no mechanical fasteners are used for joining. To maintain the panel geometry during fabrication, first stiffeners and then the skin are placed in a stitching tool for assembly prior to moving to a curing tool for consolidation in the oven. The stiffeners running in the axial direction consist of webs with unidirectional carbon fiber rods at the top of the web. AS4 carbon fiber overwraps surround the rod. The stiffeners in the lateral direction are foam-filled hats. Panels considered in the present study assumed 6-inch spacing for the rod-stiffeners and 20-inch spacing for the foam-filled hat frames. The manufacturing process is described in detail in reference 6.

While providing several unique advantages, the PRSEUS structure also presents some inherent challenges not shared by conventional metallic airframes.[7] Among these challenges are requirements for designing and manufacturing joints and repair techniques for rod-stiffened panels. While manufacturing joints and repair techniques should both be designed to be light weight and meet ultimate load requirements, they are often applied in different environments. While in a factory environment a large component with damage might be replaced in its entirety, the replacement of a large highly-integrated component with localized damage is often cost-inefficient and impractical in the operational environment. In addition, composite technology-based repair such as bonding that requires a tightly controlled environment, perishable supplies, highly skilled workers and advanced tooling to produce a reliable bond may be acceptable in a factory environment but may not be in the field. Since from a practical standpoint, basic repairs cannot depend on the availability of a factory-like environment, repair techniques applicable to PRSEUS panels in an operational environment must be developed. This paper focuses on the development, design, and analysis of bolted repairs to a damaged PRSEUS rod-stiffener. The proposed repair concept utilizes metallic fasteners rather than adhesive as the main load transfer mechanism.

Figure 1a. PRSEUS flat panel.[6]

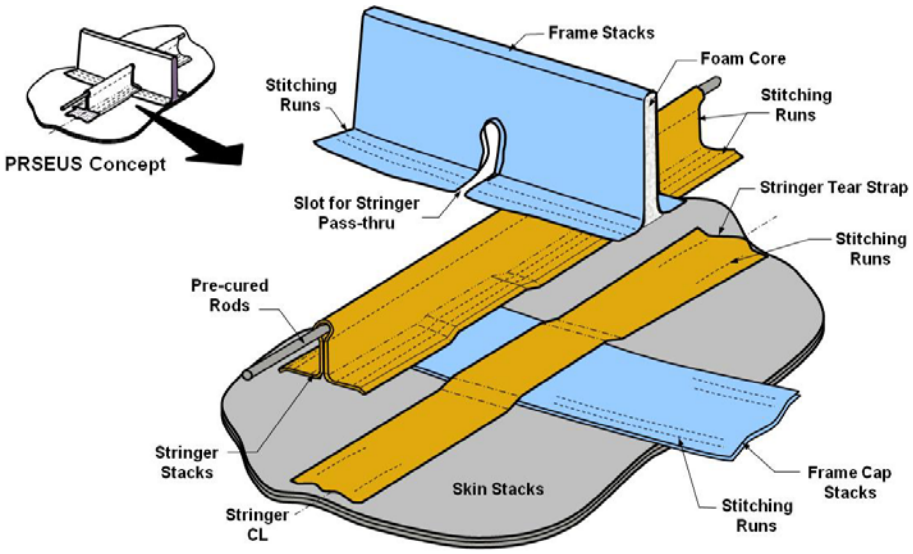

Figure 1b. PRSEUS assembly concept.[6]

This study describes the repair design concept development, finite element modeling, analysis validation and basic optimization of a repair suitable for a PRSEUS panel with severe damage involving both the skin and rod-stringer (i.e., flange, web, and pultruded rod). This repair technique is designated as "Mohawk." The repair is based on aluminum alloy components and titanium alloy fasteners so that complications related to composite repair components are avoided. The objective of the repair is to restore the load-carrying capability to that of the pristine structure. In the following sections, a comparison between test data from three tension-loaded PRSEUS panels and analytical results is presented. These results for a damaged three-stringer panel and two repaired single-stringer panels were used to validate the analysis approach. Then a repair for a three-stringer panel was designed and strains and displacements for that panel are compared to predictions for a pristine panel and the critical factors in the design are discussed.

II. Repair Objective and General Concept

First and foremost, the repair assembly was required to restore the original load carrying capability of the pristine panel while incurring the smallest weight penalty possible. In general, while not formulated as a quantitative requirement, it was also desired that the mechanics and load paths of the repaired panel resemble that of the pristine panel. Consequently, and as it will be demonstrated and discussed next, the repair design had to meet conflicting goals. On one hand, an excessively compliant repair assembly would probably lead to an insufficient load carrying capability of the repair parts and/or higher loads transferred into the undamaged sections of the panel when compared to the pristine configuration under the same loading. On the other hand, a much stiffer repair assembly would probably lead to a larger than necessary weight penalty and significantly altered load paths underutilizing the undamaged sections of the panel. An exact stiffness match of the repair assembly to compensate for the simulated damage would likely produce a repair configuration that is complicated from a manufacturing standpoint. Such a configuration would need to involve features such as continuously span-wise changing dimensions of the cross-sections of the repair parts. Secondary to the factors discussed above, there were also several established design practices to follow, including those regarding spacing requirements between metallic fasteners applied to a composite primary structure. Finally, operational factors, e.g. what is practical in an environment that the repair technique was intended for also influenced the design.

The general Mohawk repair concept was first proposed by The Boeing Company and initial exploration was conducted in a proprietary study. The Mohawk concept incorporates desired features outlined in the introduction section and is presented in Figure 2. The repair consists of two aluminum alloy upper repair pieces whose bottom ends rest on the panel's top flange surface and the vertical portions rest on web sides and wrap around the pultruded rod. The two upper pieces are bolted directly together above the rod, and bolted together through the stiffener web below the rod. The clearance between the two upper repair pieces and the pultruded rod ensures that the repair is not clamped on the rod. The lower ends of the repair components are bolted through the flanges to an aluminum alloy strap (not shown in Figure 2). The width of this lower strap is equal to or greater than the combined widths of

the two upper repair pieces, as dictated by the extent of the damage being repaired. By incorporating a stiff pultruded rod offset from the panel surface, the PRSEUS panels are designed to efficiently carry not only in-plane but also bending loads. Consequently, the Mohawk repair concept is designed such that the neutral bending axis of the three assembled repair pieces (the two upper pieces and the lower strap) coincides with the neutral bending axis of the pristine panel. This way Mohawk can transfer combined in-plane and bending loads in a similar fashion as the pristine panel.

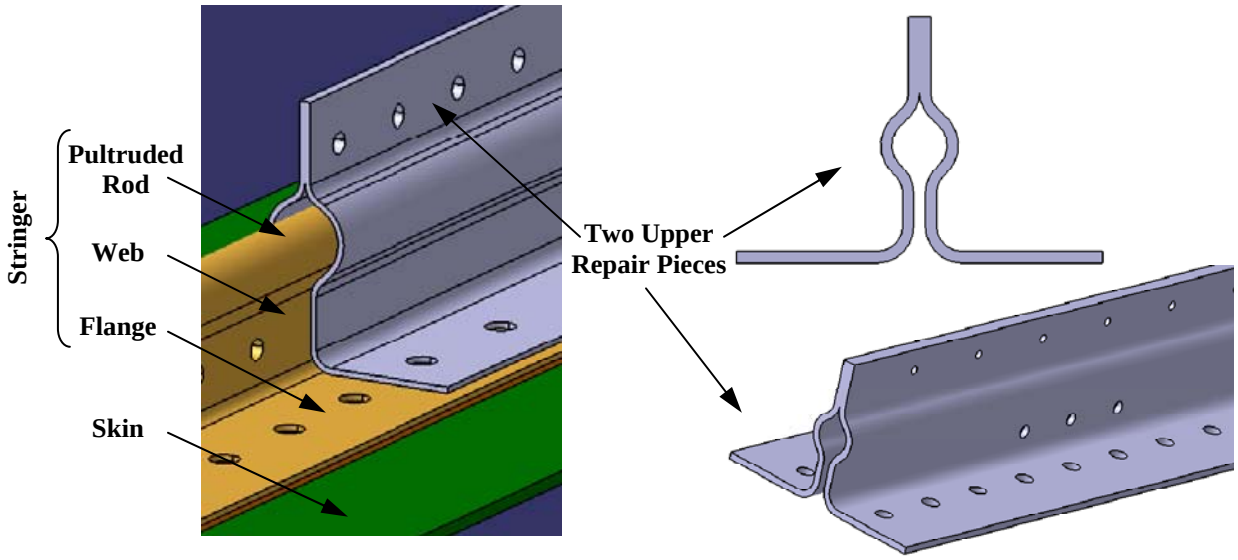

Figure 2. General Mohawk repair concept.

III. Repair Analysis Methodology and Validation

Validation of the analysis approach was conducted by analyzing single-stringer and three-stringer PRSEUS panels. This validation was necessary to instill confidence in the methodology for predicting behavior of PRSEUS damaged structure and the Mohawk repair. The commercial finite element (FE) package Abaqus[8] was used in the analyses being presented. The Abaqus/Standard (implicit) solver supporting both material nonlinearity and geometrically nonlinear behavior was utilized. Several FE models were developed in the course of the study based on the same methodology.

A. Single-stringer panel

The first configuration used to validate the FE modeling was a single-stringer repaired panel presented in Figure 3. This PRSEUS panel was fabricated and tested by Boeing. Due to the proprietary nature of the test data, results used in the FE analysis validation effort are non-dimensionalized as a ratio between the test and analysis results. The single-stringer panel's damage was limited to the pultruded rod and web, as presented in Figure 4a as a circular cut-out in the stringer. This type of damage, limited to the inner (substructure) side of the panel, is representative of an impact damage incurring during the manufacturing process or inspection. The single-stringer panel cross-section with the assembled Mohawk repair including the two upper repair pieces and the lower strap is presented in Figure 4b. Strain gauge data acquired during the tension test was used to validate the FE analysis model of the PRSEUS panel and Mohawk repair, including the joints between the composite panel and metallic repair parts.

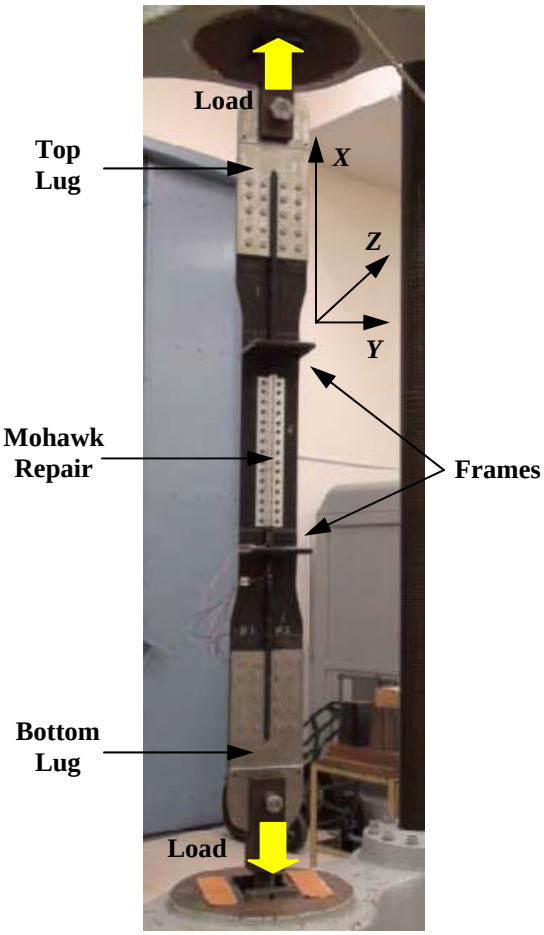

Figure 3. Mohawk repair assembly installed on a single-stringer PRSEUS panel.

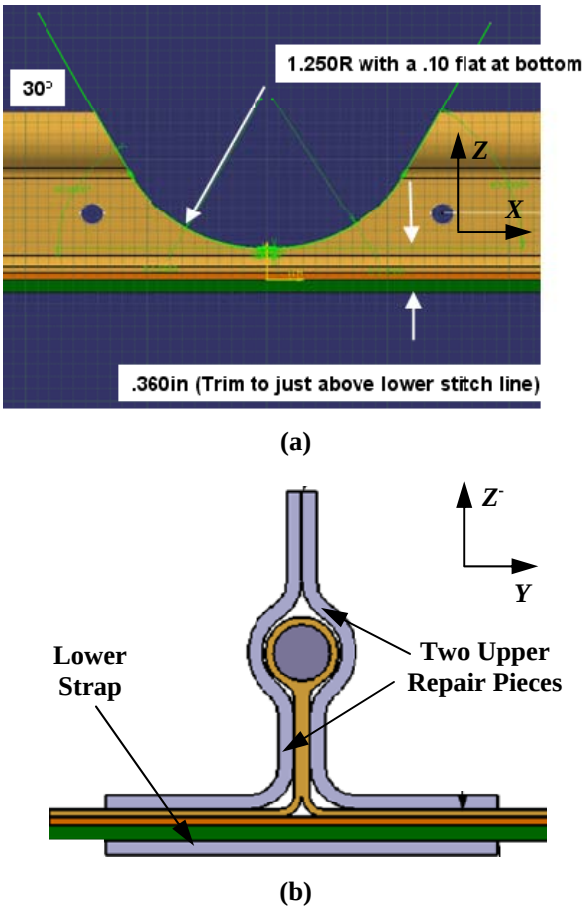

Figure 4. Single-stringer PRSEUS panel (a) simulated rod and web damage, (b) repair assembly cross-section.

The length of the test section of the panel between the foam-core frames was 20 inches. The width of the test section was 6 inches. i.e., equal to a typical spacing between rod-stringers in multi-stringer panels. The lugs visible in Figure 3 were designed to impose a uniform in-plane displacement across the panel's width at both ends of the test section. The frame height measured from the outer (smooth) side of the panel was 6 in. and the foam used in the frame's core was 0.50-in. thick. The height of the stringer was 1.49 in. with the rod center offset by 1.25 in., both measured from the smooth side of the panel. The rod diameter was 0.375 in. The lamination stacking sequences of different sections of the panel are presented in Table 1. Each stack was orientated either in the *X*-axis direction, parallel to the rod-stiffener, or in the *Y*-axis direction, perpendicular to the rod-stiffener as shown in Figure 3. The two upper repair pieces were made of 0.10-in. thick aluminum alloy 7050-T7451. The lower strap was made of 0.09-in. thick aluminum alloy 7075-T6. Since the material properties of the aluminum alloys are very similar, in this study the 7075-T6 properties are assigned to all aluminum alloy components. The fasteners attaching repair pieces to the panel are assumed to be made of the titanium alloy Ti-6Al-4V. The material properties used throughout the current studies are listed in Table 2. Per typical aircraft certification requirements[9] a metallic structure is expected to remain in the elastic regime below the limit load, but the plastic regime is permitted at the ultimate load. Consequently, aluminum alloy elastic-plastic material properties, modeled as a bi-linear stress-strain relationship, were utilized in the Mohawk repair assembly. All composite material properties were modeled as elastic only. Titanium alloy fasteners were not permitted to exceed their yield stress values.

Table 1. Single-stringer panel lamination stacking sequence.

Panel's Component	Stack Orientation from the Smooth Side of the Panel, 0° Along the *X*-Axis (Panel's Length)
Skin	(0, 0)
Skin w/Flange	(0, 0, 0, 0)
Skin w/Frame Cap	(0, 0, 90, 90, 90)
Skin w/Flange and Frame Cap	(0, 0, 90, 0, 0, 90, 90)
Web	(0, 0)
Frame	(0, 0, foam, 0, 0)*

*0° Along *Y*-Axis (Frame's Length)

Table 2. Material properties.

Material	E_1, Msi (H_1, ksi)	E_2, Msi (H_2, ksi)	ν_{12}	G_{12}, Msi	Tensile Ultimate Strain, μin./in.	Tensile (Yield) Strength, ksi
Rod Toray T800/3900-2B	16.1		0.30	6.19	16,800	390.0
AS4-VRM34 (Stack Properties)	9.74	4.86	0.40	2.37	10,000	105.1
Aluminum Alloy 7075-T6	10.3 (60.5)	10.3 (60.5)	0.33	3.87		78.0 (69.0)
Foam Core Rohacell 110WF	0.021	0.021	0.32	0.008		0.441
Titanium Alloy Ti-6Al-4V Grade 5	16.5	16.5	0.342	6.38		138.0 (128.0) Shear Strength 79.8

A FE model of the single-stringer panel test specimen was developed using S4R5 shell elements to model the panel's skin, flanges, frames, web and Mohawk repair components, B31 beam elements to model the pultruded rod, and CONN3D2 connector elements to model the fasteners attaching the Mohawk repair. The through-the-thickness stitches were not modeled in the analysis because previous studies[10] have shown that accurate global analysis results can be obtained without such a high-fidelity modeling. The boundary conditions (BCs) were modeled as clamped at one end and clamped with a uniform in-plane displacement at the opposite end. These BCs were applied over the area where the lugs were bolted to the composite specimen ends as can be seen in Figure 3.

Representative repaired panel FE results are presented in Figure 5 for an applied in-plane displacement of 0.10 in., which results in the total in-plane reaction force of 36.24 kip. Two panels were tested in tension until their ultimate loads were reached while strain gauge and displacement data was recorded. Since the damage occurring at failure was not modeled in the present studies, strain measurements at loads less than failure initiation were used to validate the FE analysis results. Seven strain gauge measurements were selected for the comparison and their locations are presented in Figure 6. Locations 2 and 5 are on the upper repair and the lower strap, respectively. Locations 3 and 4 are on the panel's skin on either side of the damaged rod and web location. Gages 2, 3, 4, and 5 are located mid-length. Finally, locations 6, 9 and 10 are located 12.85 in. away from the mid-length location (or 2.5 in. from the outer surface of the frame), i.e. outside of the repair region, and provide the far-field strain values. Therefore, a comprehensive survey of the FE analysis and test results was accomplished. Since the test data was proprietary, the strain level comparison is presented as a ratio of the FE analysis result over the test result. The ratios for each of these gauges are presented in Table 3 both test specimens for the load level of 36.24 kip, corresponding to the displacement field of Figure 5 and the agreement is considered favorable. These results indicate that the specimens differ from each other by as much 12 percent in some locations and the analysis differs from the test data by no more than 17 percent in some locations and is within 2 percent in others. This validation indicates that all aspects of the exercised FE modeling techniques are adequate to predict the behavior of the Mohawk repair for a design study.

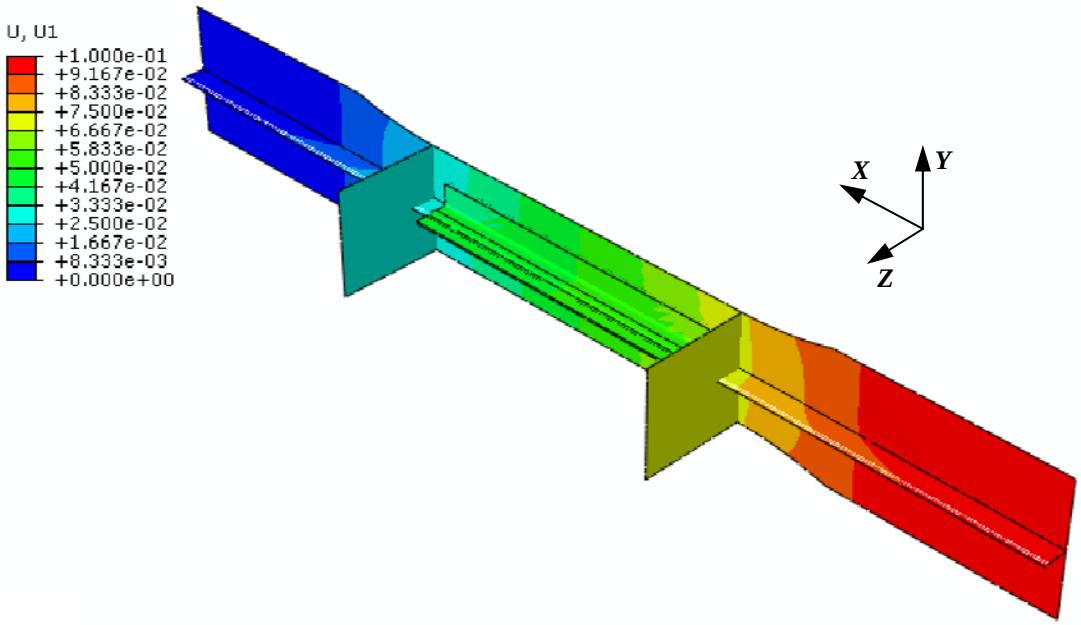

Figure 5. Predicted single-stringer repaired PRSEUS panel axial displacement in inches.

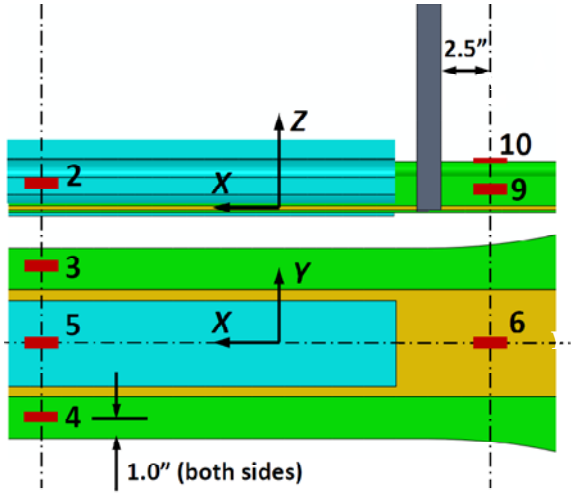

Figure 6. Single-stringer panel strain gauge locations.

Table 3. Single-stringer panel FE analysis versus test data strain ratios comparison at 36.24 kip loading.

Strain Gauge Location	Strain Ratio	
	Test Article 1	Test Article 2
2	1.15	1.15
3	0.89	0.99
4	0.99	0.87
5	0.98	0.98
6	1.10	1.17
9	0.88	0.93
10	0.94	0.84

B. Three-stringer panel

Next, a three-stringer panel was considered in the validation effort. The test data for a three-stringer configuration was available from a tension test of a panel with the saw-cut damage, as presented in Figure 7. The objective of the test was to demonstrate the damage arresting capabilities of the PRSEUS structure,[11] which is not in the scope of the present work. Nevertheless, the data acquired from that panel test before the damage propagation started was valuable in the FE modeling validation efforts. The type of the initial three-stringer panel damage, extending not only through the pultruded rod and web but also including the flange and skin, is representative of a worst case of operational damage where a penetration from the outer (smooth) side of the panel by a foreign object such as a fan blade is encountered. The three-stringer panel test data was used to validate the modeling of the damaged panel without the installed repair, an aspect of the FE modeling validation which was not possible using the single-stringer test results. This way both the repair technique and damaged panel FE modeling accuracy were assessed.

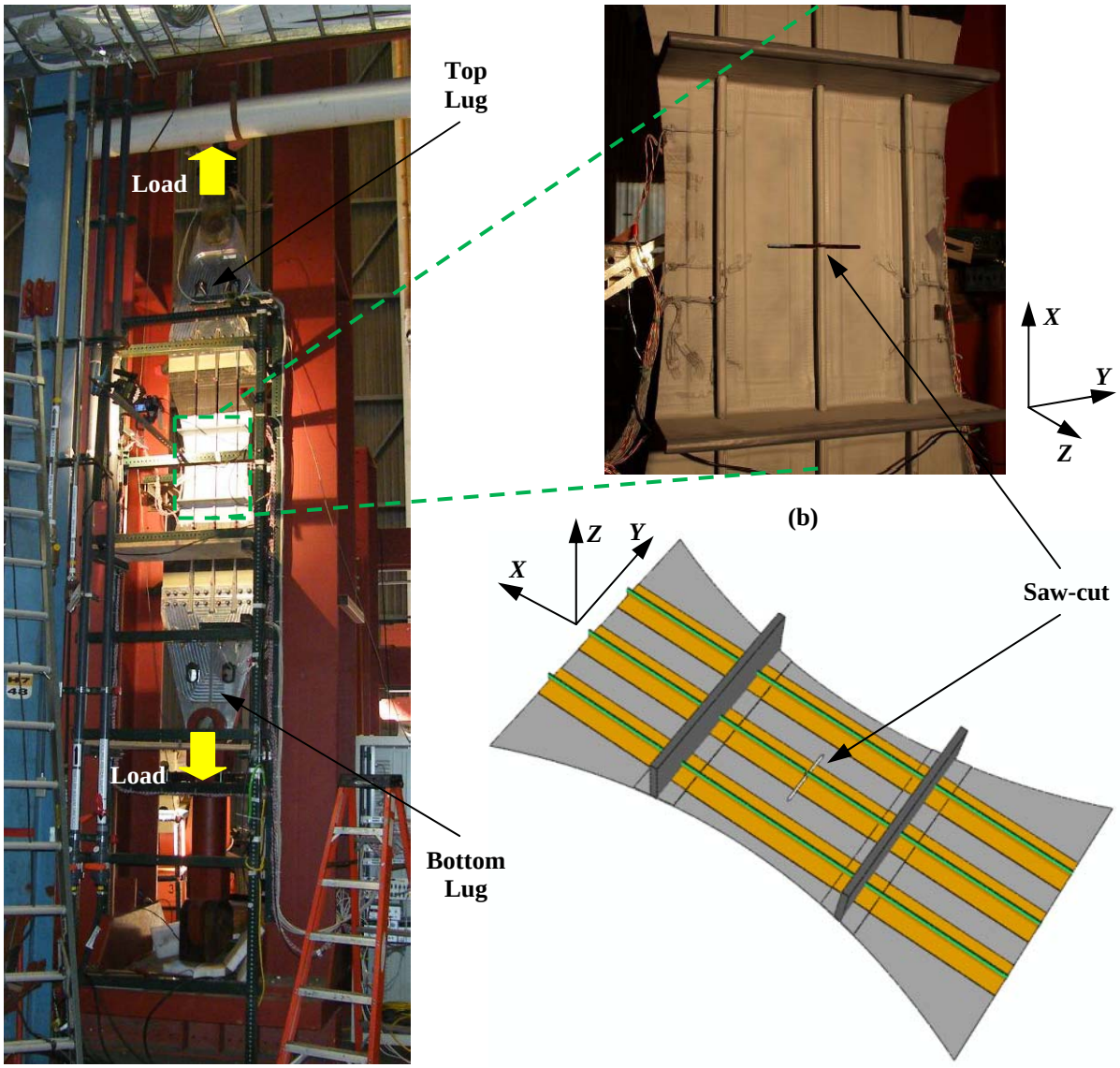

Figure 7. Three-stringer PRSEUS panel with saw-cut damage (a) test specimen in fixture, (b) test section close-up, (c) FE model.

The three-stringer panel total specimen length including lugs, as shown in Figure 7a, was 154.4 in. (142.0 in. pin-to-pin), but only the dog-bone test section measuring 50.0 in. was modeled using FE, as presented in Figure 7c. The span of the centrally located saw-cut was mid-bay to mid-bay (6 inches) and its width was 0.25 inches. Consequently, the pultruded rod, web, flange, and skin were severed, which represented a qualitative difference from the single-stringer panel damage which was limited to the rod and web only. Analysis of the three-stringer panel, therefore, presented an opportunity to verify that the FE modeling technique was adequate to ensure redistribution of the loading from the damaged section to the adjacent stringers. The lugs were assumed to impose a uniform in-plane displacement in the panel at the two cross-sections where the panel width begins to reduce to achieve the dog-bone shape. Therefore, the BCs applied in the analysis were clamped at one end, and clamped with a uniform axial in-plane displacement at the opposite end. Assuring proper load distribution in the damaged multi-stiffener panel was a necessary pre-requisite to confidently analyzing a repaired panel. The three-stringer panel lamination stacking sequences are presented in Table 4. Note, that the two 0° skin stacks used in the single-stringer panel are replaced in the three-stringer panel with a single 90° stack. The remaining dimensions corresponding to stringers and frames are identical to the ones of the single-stringer panel.

Table 4. Three-stringer panel lamination stacking sequence.

Panel's Component	Stack Orientation from the Smooth Side of the Panel, 0° Along the *X*-Axis (Panel's Length)
Skin	(90)
Skin w/Flange	(90, 0, 0)
Skin w/Frame Cap	(90, 90, 90, 90)
Skin w/Flange and Frame Cap	(90, 90, 0, 0, 90, 90)
Web	(0, 0)
Frame	(0, 0, foam, 0, 0)*

*0° Along *Y*-Axis (Frame's Length)

As for the single-stringer panel, the three-stringer panel was discretized using S4R5 shell elements for all of its components except the pultruded rods which were model using B31 elements. The FE model presented in Figure 7c has 27,686 nodes and 28,050 elements (27,300 S4R5 and 750 B31) for total of approximately 150,000 degrees-of-freedom (DoF).

The strain results were compared with the test data at six selected mid-length locations, four on the outer (smooth) side of the panel and two on the inner (substructure) side of the panel, as presented in Figure 8. For consistency with the discussion of the single-stringer panel, the FE analysis versus test strain ratios are presented in Table 5. The comparison indicates that the test and analysis results differ by no more than 12 percent at any of these locations. Furthermore, the strain ratios presented in Table 3 for the single-stringer panel and in Table 5 for the three-stringer panel are of a similar range. Therefore, the FE modeling techniques for the range of panel sizes and repairs considered were deemed accurate and suitable for use in further studies.

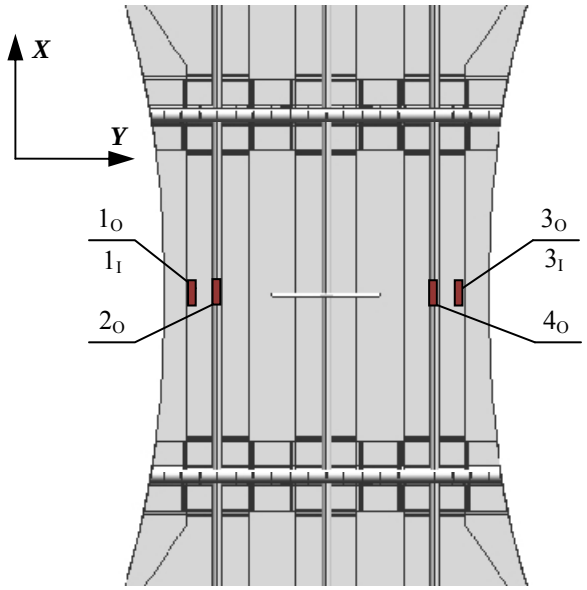

Figure 8. Three-stringer saw-cut panel strain gauge locations.

Table 5. Three-stringer panel FE analysis versus test data strain ratios comparison at 20.53 kip loading.

Strain Gauge Location‡	Strain Ratio
1_O	1.12
1_I	1.02
2_O	1.00
3_O	0.95
3_I	0.95
4_O	0.96

‡Stain gauge locations designated with N_O in Figure 8, where N is a number, correspond to measurements obtained on the outer (smooth) side of the panel; strain gauge locations designated with N_I are collocated with N_O gauges but on the inner (substructure) side of the panel.

IV. Repair Design

Once the FE analysis validation effort was successfully completed, the repair assembly design task was initiated and two additional FE models were developed to support the repair design and analysis. First, the same three-stringer panel used in the validation effort was modeled in a pristine configuration to assess the mechanics and load carrying capability of such a panel. The results from this analysis were used as a baseline for comparison to the repaired panel, as the repair was intended to restore the original load carrying capability. Test results from the afore-

mentioned tension test of the crack-arresting panel,[11] however, were also used to guide the repair assembly load carrying capability requirements. Finally, the three-stringer repaired panel itself was modeled. The same panel material properties, dimensions and modeling techniques used for the saw-cut panel are used for the pristine and repaired three-stinger panel. As previously modeled in the single-stringer repaired panel, aluminum repair pieces are attached to the panel with titanium fasteners represented with the CONN3D2 connector elements. The same material properties used for the single-stringer panel repair assembly are also applied to the three-stringer panel repair assembly.

Several configurations of the Mohawk repair concept were explored and the most structurally efficient and manufacturable solution identified thus far is presented in Figure 9. While the numerous repair configurations considered are not described in detail herein, the parameters that were varied in the process of determining the current repair configuration are listed and briefly discussed. The initial selection of parameters which were considered as the repair design variables included: (1) thicknesses of the repair pieces, (2) length of the two upper repair pieces, (3) length of the lower strap at the center, (4) length of the lower strap side edges, (5) panel conditioning in the vicinity of the saw-cut damage such as gradually tapering the pultruded rod at its termination, and (6) number and spacing of fasteners. Optimal selection of these parameters, in general, will vary with the extent and location of the damage.

In the design of the repair of the saw-cut three-stringer panel, several specific conclusions were reached. The thicknesses of the repair pieces used in the single-stringer panel preserved the location of the neutral bending axis of the repaired section and these thicknesses were adequate for the load redistribution required in the three-stirnger panel so these thicknesses remained unchanged in the repair of the three-stringer panel. Namely, the thickness of the two upper pieces was 0.10 in., and the thickness of the lower strap was 0.09 in. This thickness could be maintained even though only the web and rod were damaged in the single-stringer panel while the flange and skin were also damaged in the three-stringer panel.

Since containing the repair between the frames would reduce the repair complexity and simplify the installation, it was considered advantageous to contain the repair length within a single panel bay. This feature was particularly important for the upper repair pieces, as their extension beyond the damaged bay would affect the integrity of the two frames. As seen in Figure 9a, this restriction was successfully incorporated in the current repair design. The two upper pieces of the repair attached to the severed stringer are very similar to those of single-stringer repair. Their original height of 2.11 in. used in the single-stringer panel is maintained. The most noticable difference is the extension of the portions of the upper repair pieces which attach to the flanges. These sections of the upper repair assembly terminate before the frame caps in the single-stringer panel but extend over the frame caps in the three-stringer repair, permitting additional fasteners in these areas. Since these sections of the PRSEUS panel comprise of six laminate stacks rather than only three in the flange areas away from the frame caps, the bottom section of the upper repair pieces is formed such that it accounts for the corresponding thickness differential of 0.156 in., as seen in the close-up section of Figure 9a surrounded by the red dashed line. Note that, consistent with the single-stringer panel repair, the combined width of the two assembled upper repair pieces at their bottom edge is limited to approximately the width of the flange, i.e. 2.7 in., as they are not intended to cover the full extent of the skin damage. The vertical portions of the two upper repair pieces parallel to the stringer's web are also slightly extended to accommodate additional fasteners. Finally, machined slots separate each upper repair piece into three segments at each end. These slots separate the end cross section into a horizontal section resting on the top of the flange, a vertical section resting against the web, and a rounded section around and above the rod, as seen in the close-up insert in Figure 9a. The three distinct sections mentioned above have their respective total lengths of 18.8 in., 16.0 in., and 15.0 in. The distance between the tips of the machined slots, i.e. the length of the upper repair pieces without the machined slots, is equal to 11.4 in. The machined slots are introduced to increase compliance of the upper repair pieces close to their ends. A discussion of the influence on these slots on load distributions is presented in a following section.

The lower strap of the repair, presented in Figure 9b, has dimensions of 20.0 in. by 12.0 in., i.e. it is longer and wider than the lower strap used in the single-stringer repair. The width of the strap is increased so it can cover more than the full width of the skin damage and, as a result, also be attached to the side flanges. The length of the strap is increased to permit its end edges to also be attached to the frame caps rather than to the flanges only. To simplify the design the strap has a rectangular, rather than a more complicated shape. More importantly, since the portion of the vehicle which contains this repair is assumed to be pressurized, an adhesive bond is needed to contain the pressure. The rectangular shape of the lower strap minimizes the length of an adhesive bond between the strap and the panel that is not accompanied by fasteners (fasteners are not allowed in the unstitched areas, such as skin, but are allowed in the stitched areas, such as flanges and frame caps). Note, that since an adhesive bond is for pressurization purposes only, it was not considered in the current FE analyses as a part of the primary load carrying

mechanism. Further note, that a single-stack skin is very compliant and its deformation increases at locations farther away from the stiffer panel components, such as frame caps, and closer to the discontinuity (saw-cut). Therefore, it was anticipated (though not verified) that the adhesive bond will be least stressed with the current lower strap configuration. Finally, since the fasteners which are used to attach the lower strap to the side flanges and frame caps must not cause crushing damage to upper surfaces in these areas, protective washers distributing the load over a larger area will be used in these locations.

Next, several configurations of the severed pultruded rod were considered. Solutions ranging from an abrupt termination, as in the case of the crack-arresting panel, to gradual tapers with different length and location were investigated. While an extremely gradual taper was generally found desired, a taper length exceeding 3 in. was considered impractical to achieve in the operational environment. Therefore, effectively the rod taper sensitivity analysis was limited to the investigation of the position of the taper relative to the saw-cut damage. Eventually, the design of terminating the rod 3 in. from the middle of the saw-cut was selected.

The main section of Figure 9a shows also 1-in. diameter holes drilled at the tips of the saw-cut damage. These holes are intended to reduce stress concentrations in these regions. A practical benefit of the stop-drills may be also to help visually detect whether the damage exhibits tendency to propagate beyond the condition at which it was detected and repaired.

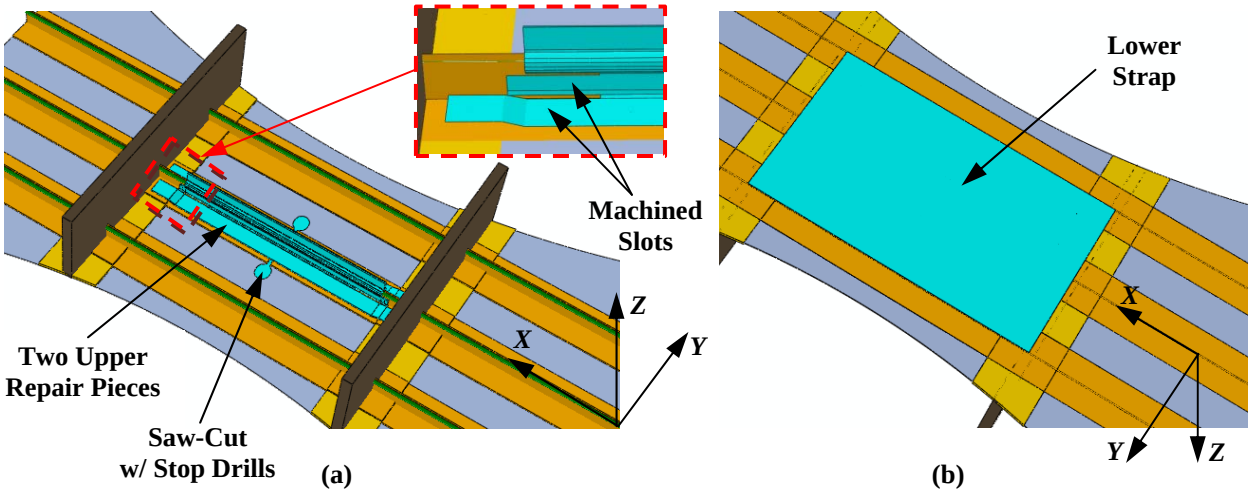

Figure 9. Three-stringer repaired PRSEUS panel (a) substructure side, (b) smooth side.

The fastener pattern design was also guided by the original fastener pattern used in the single-stringer panel repair and is presented in Figure 10 with the black points. Fasteners attaching the repair assembly to the horizontal (the *X*-*Y* plane) sections of the panel are primarily intended to transfer the loads from the severed flange to the repair assembly. The row of fasteners installed in the *X*-*Z* plane below the damaged rod attaches both upper repair pieces to the severed web. Since the severed rod on top of the severed web is not directly attached to the repair assembly, as such an attachment is not feasible because the rod must not be drilled through or clamped on, these fasteners are effectively exposed to the loads transferred from the very stiff rod through a more compliant web into the repair assembly. Finally, the row of the fasteners connecting only the two upper repair pieces above the severed rod is primarily for stability of the upper repair assembly and does not participate in the transfer of loads from the panel to the repair assembly.

Each fastener group labeled in Figure 10 is followed by the fastener diameter used in this specific group. General guidelines for the fastener pattern in a composite structure followed in the present work required that fasteners be at least four diameters from each other and at least three diameters plus 0.06 in. from any free edge. The two upper repair pieces are attached through the severed flange to the lower strap using 32 0.25-in. diameter fasteners (eight in front of the center stringer to the left of the saw-cut and eight in front of the center stringer to the right of the saw-cut are visible in Figure 10a, while their symmetric counterparts behind the center stringer are only visible in Figure 10b). The seven fasteners in each panel quadrant that are closest to the saw-cut are spaced 1.0 in. apart, i.e. four times their diameter. The distance between the edge of the saw-cut and the first fastener is 0.81 in., i.e. three times its diameter plus 0.06 in. The four fasteners closest to the frames are penetrating the frame cap and flange crossings which are thicker than the flange alone. They are located 1.85 in. away from the next fasteners to

place them in the middle of the thicker section of the panel with equal spacing from the frame and the thickness discontinuity. Twenty 0.19-in. diameter fasteners, ten on each side of the saw-cut, are used to attach the two upper center repair pieces together through the web. The spacing of these fasteners is 0.76 in., i.e. four times their diameter. The distance between the edge of the saw-cut and the first fastener is 0.63 in, i.e. again three times its diameter plus 0.06 in. With the exception of the fasteners closest to the frames, the spacing of 1.0 in. is also used to attach the lower strap to the side flanges. The total of 16 0.25-in. diameter fasteners is used on each side of the panel (only one row of these fasteners is visible in Figure 10a, while both fastener rows are seen in Figure 10b). Since the saw-cut does not extend to the proximity of the side flanges, these fasteners do not have an extended spacing at the panel's mid-length location. The four fasteners closest to the frames are again penetrating the frame cap and flange crossings which, as mentioned before when discussing the center 0.25-in. fastener arrangements, are thicker than the flange alone. These fasteners are located 2.28 in. away from the next fasteners (spaced with 1-in. increments) to place them in the middle of the thicker section with equal spacing from the frame and the thickness discontinuity. Additionally, eight 0.25-in. fasteners, two in each quadrant of the panel, are attaching the bottom strap to frame caps between the center and side flanges. Widthwise, these fasteners are aligned with the far 0.25-in. fasteners penetrating the frame cap and flange crossings. The distance between the fasteners penetrating the frame cap and flange crossing and the neighbor ones penetrating only the frame cap is 1.7 in. Finally, the two upper repair pieces are connected together above the pultruded rod with 18 0.16-in. diameter fasteners spaced at 0.8 in., or five times their diameter. Note, that the latter fasteners and the fasteners attaching the lower strap to the side flanges and frame caps work as single-shear fasteners, while all other work as double-shear fasteners, which is in general considered a preferred condition.

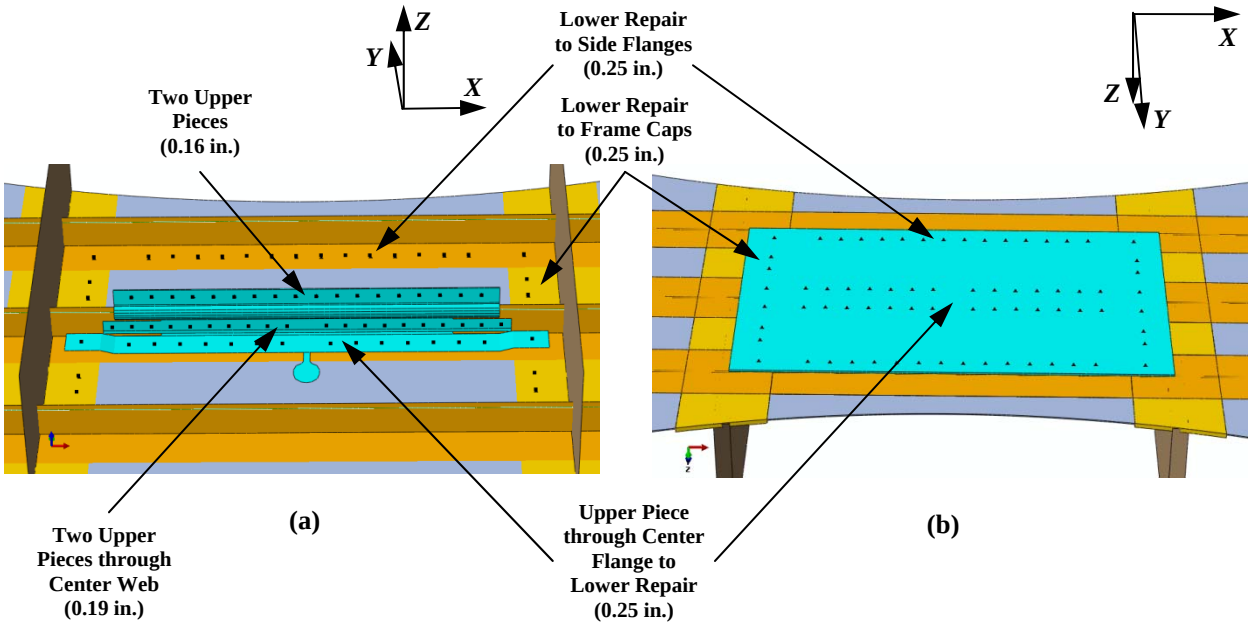

Figure 10. Location of fasteners viewed from (a) substructure side, (b) smooth side. Dimensions represent fastener diameter.

V. Detailed Analysis Approach

As mentioned before, Abaqus fastener modeling based on connector elements was utilized.[8] The connector element-based fastener modeling requires determination of their three translational and three rotational stiffness values. In the initial single-stringer panel analyses only approximate and, consequently, over-estimated fastener stiffness values were used, where their response approached rigid kinematic constraints. This approach was appropriate at a low, survey-type loading level, where the localized effects associated with fastener attachments were not investigated in detail. A refined fastener stiffness estimation was introduced to the three-stringer repaired panel modeling as the model was intended for investigation of the ultimate load carrying capability, which was likely to be limited by fastener joints. The fastener stiffness values were computed based on the guidelines provided in ref. 12, i.e.

$$K_{T(1)}=\frac{EA}{L} \tag{1}$$

$$K_{T(2,3)}=\frac{GA_S}{L} \tag{2}$$

$$K_{R(1)}=\frac{GJ}{L} \tag{3}$$

$$K_{R(2,3)}=\frac{EI}{L}+\frac{GA_SL}{3} \tag{4}$$

where

$$A=\frac{\pi d^2}{4} \tag{5}$$

$$A_S=\frac{A}{\alpha_s} \tag{6}$$

$$I=\frac{\pi d^4}{64} \tag{7}$$

$$J=\frac{\pi d^4}{32} \tag{8}$$

and the local direction *1* is aligned with the fastener's length. Ref. 12 also provides a guidance to estimate the stiffness of the local structure, which should not be overwhelmed by the fasteners' stiffness $K_{T(2,3)}$, as

$$S=\frac{t_sE_sE}{E_s+E} \tag{9}$$

where values of E_s for non-isotropic structure were computed according to the rule of mixture weighted by the thickness components of t_s, i.e.,

$$E_s=\frac{1}{t_s}\sum_i E_it_i. \tag{10}$$

Individual summation components in Eq. (10), in general, correspond to composite stacks with different orientations and aluminum repair components. Therefore, values of E_s computed in directions *2* and *3* may be different. Stiffness values computed through Eqs. (1-8) and, where applicable, verified not to exceed the local stiffness of Eq. (9) are presented in Table 6 for the three distinct diameters of the fasteners used in the repair. All the 0.16-in. and all the 0.19-in. fasteners are of equal length resulting in the same stiffness values for a given fastener diameter. Stiffness values for the 0.25-in. fasteners are presented as a range, as the length, and consequently stiffness values, vary with their location.

Table 6. Fastener stiffness values.

d, in.	$K_{T(1)}$, lb-f/in. $\cdot 10^6$	$K_{T(2,3)}$, lb-f/in. $\cdot 10^6$	$K_{R(1)}$, lb-f in. $\cdot 10^3$	$K_{R(2,3)}$, lb-f in. $\cdot 10^3$
0.16	0.634	0.464	1.978	8.834
0.19	0.660	0.430	2.587	16.72
0.25	0.989-1.979	0.451-0.654	4.696-6.814	35.25-44.17

The fastener definition in the single-stringer panel, in terms of their sizes and locations, was already prescribed and not subject to modifications. Since several fastener arrangements were to be considered for the three-stringer panel, a FE modeling technique that minimizes effort associated with modifying fastener patterns was employed. The connector elements used to model fasteners in the single-stringer panel were defined utilizing the nodes of the panel and the repair assembly. Maintaining this type of fastener modeling would imply re-meshing a significant portion of the FE model each time the fastener pattern is modified. To mitigate this inconvenience, a mesh-independent fastener modeling offered by Abaqus[8] FE code was adopted. The most important features of this approach are highlighted in Figure 11 and Figure 12.

As shown in Figure 11, Abaqus permits definition of surfaces that are being attached by fasteners and definition of a positioning point in the proximity of these surfaces. A normal to the surfaces that are being connected and passing through the positioning point can be defined and points on the surfaces penetrated by this line become the fastening points. The load between the fastener and each surface is being distributed over the area within the radius of influence, as presented in Figure 12 with grey circles. This radius of influence is defined by the fastener radius. Consequently, the load from a fastener is distributed over all the elements within the radius influence and subsequently used to compute corresponding reaction forces at all the nodes associated with the elements within the radius of influence. This way not only a more realistic, distributed rather than point load distribution being introduced, but also relocation of fasteners and/or modifying their diameters does not involve any modification of the mesh associated with parts being fastened. Effectively, only coordinates of the positioning point and one parameter defining the diameter of the fastener needs to be changed.

As illustrated in Figure 12, the physical number of fasteners in the model is not necessarily equal to the number of the connector elements used to model them. When only two parts are connected with a fastener, one connector element represents one fastener, as seen on the right hand side of Figure 12. Such a configuration is the case, e.g., for the top row of 0.16-in. fasteners above the pultruded rod joining together the two upper repair pieces, shown in Figure 10a. When a single fastener is attaching together three parts, two connector elements are needed in a FE model, each connecting the two parts located next to each other, as seen on the left hand side of Figure 12 where one connector element attaches fastening points A and B and one connector element attaches fastening points B and C. Such a configuration is the case, e.g., for the row of 0.19-in. fasteners connecting the two upper repair pieces and the web in between them, shown in Figure 10a.

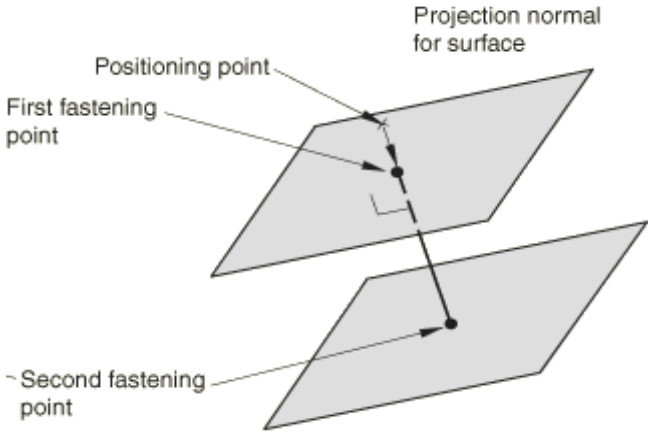

Figure 11. Fastening points definition in Abaqus FE code.[8]

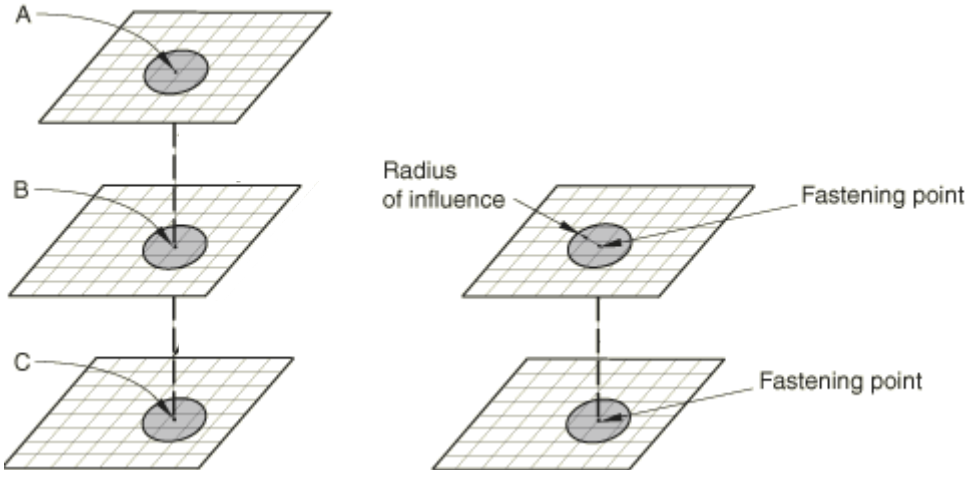

Figure 12. Fastener two- and three-part joint modeling in Abaqus FE code.[8]

To summarize the FE modeling effort, the overall model statistics are given. The number of elements in the FE models of the pristine and saw-cut panels is the same and the number of nodes in the two models is also nearly identical. The current repaired panel FE model has 38,891 nodes (i.e. 11,205 more than the saw-cut model) and 36,564 elements (i.e. 8,514 more than the saw-cut model). The additional elements are 8,352 S4R5 elements used to model the three aluminum repair pieces (i.e., the two upper center pieces and the bottom strap) and 162 CONN3D2 connector elements used to model the 108 fasteners in the model.

Finally, a stress-strain analysis approach which specifically pertains to fastener joints analysis and design is introduced and related FE analysis post-processing considerations are discussed. The concept of bearing stress-bypass strain analysis applicable to fastened joints can be summarized as follows. Consider a free body diagram of a structure surrounding a fastened joint under a uniaxial tension loading, as presented in Figure 13, which is a condition representative of the repaired panel configuration. A bypass load results in a bypass strain, ε_{BP}, that can be obtained from a FE analysis. Averaged strains obtained from the elements on the bypass side of the fastened joint (i.e. below the fastener hole in Figure 13) can be used and the presence of a hole to accommodate the fastener can be neglected.[13] Also according to ref. 13, the bearing stress, σ_P, can be computed as

$$\sigma_B = \frac{P_B}{t_s d} \tag{11}$$

where in the present analysis the bearing force, P_B, was obtained from the FE connector element output associated with each fastener. The bearing stress and bypass strain values, obtained as just described, can be plotted for a given location in a fashion presented in Figure 14 with sample blue and green data points. Based on proprietary test data, two distinct failure mechanisms can occur dependent on relative magnitudes of the bearing stress and the bypass strain.[13,14] These are net section failure and bearing failure. While the bearing failure is independent of the bypass strain level as indicated by the vertical green dashed line, the maximum bypass strain allowable depends on the bearing stress level as presented with a sloped blue dash line. If a particular operating point is contained under the two dashed lines failure will not occur. The margin of safety can be estimated by plotting a straight line through the origin of the coordinate system and a data point until it intersects with either dashed line. The ratio of the total line length until the intersection with a dashed line relative to the distance of a given point from the origin produces the margin of safety value when the value of one is subtracted from it.

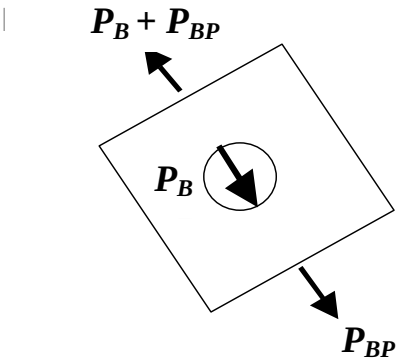

Figure 13. Free-body diagram of a fastened joint under uniaxial tension loading.[13]

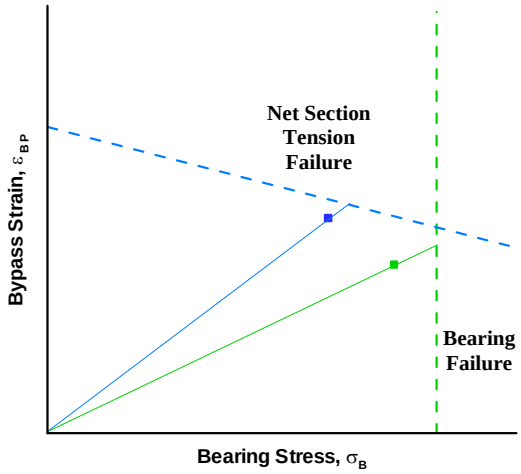

Figure 14. Bearing stress-bypass strain typical trend lines of a composite material allowables under tension loading.[14]

VI. Pristine and Repaired Three-Stringer Panel Results Comparison

Based on the pristine panel simulation and available test results a limit load of 146 kip and an ultimate load of 219 kip were assumed for the current studies. These two loadings corresponded to a uniform axial end displacement of 0.265 in. and 0.397 in., respectively, for the pristine panel and 0.241 in. and 0.361 in. for the repaired panel. Both results pointed to a nearly linear relationship between the enforced displacement and force loading. Note that this observation does not imply a linear relationship between strains and/or stresses and applied force or displacement

loading, especially when a localized behavior is considered. As it will be discussed later in this section, some portions of the repair assembly exceeded yielding stress levels, so that a nonlinear elastic-plastic material behavior was triggered. Since only small sections of the repair assembly were affected by the nonlinear material behavior, the overall load versus displacement relationship did not significantly depart from a linear trend line. For both limit and ultimate loadings, the enforced displacement values for the pristine panel were found to be only approximately 9% larger than the ones obtained from the repaired panel analyses, pointing to the repair panel being overall slightly stiffer than the pristine one. This result is not surprising, as the repair design was intended to restore the pristine panel condition.

The in-plane and out-of-plane displacement fields of the pristine and repaired panels subjected to the ultimate in-plane loading of 219 kip are shown in Figure 15 through 18. It is seen in Figure 15 and 16 that the in-plane displacement fields are very similar with fairly uniform in-plane displacement distributions across the width of the panels away from the side edges of the dog bone contours. Noticeably however, for the repaired panel presented in Figure 16, the in-plane displacement in the proximity of the left frame is slightly smaller in the vicinity of the center stringer than it is in the vicinity of the two side stringers while the in-plane displacement in the proximity of the right frame is slightly larger in the vicinity of the center stringer than it is in the vicinity of the two side stringers. This result is due to the slightly higher stiffness of the repaired center stringer relative to the two pristine side stringers, as discussed before.

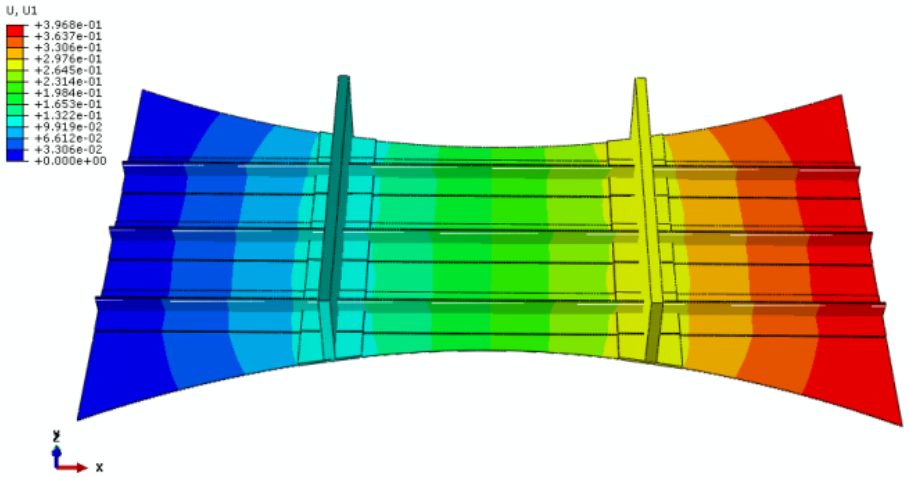

Figure 15. Pristine panel in-plane displacement, in.

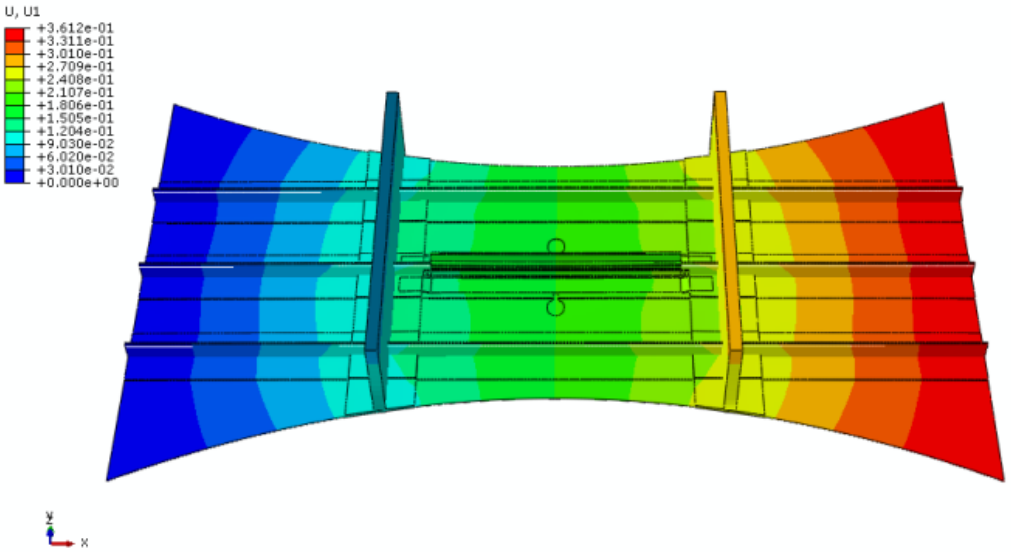

Figure 16. Repaired panel in-plane displacement, in.

The out-of-plane displacements, presented in Figure 17 and 18 for the pristine and the repaired panels, respectively, differ more significantly in terms of both displacement distribution and magnitude than the in-plane displacements. The maximum out-of-plane displacement is 0.034 in. for the pristine panel and 0.117 in. for the repaired panel, and both are marked as points A in their respective plots. While the relative difference of the out-of-plane displacement is large, their overall magnitudes are small when compared to the in-plane displacement values. In case of the repaired panel, the absolute maximum displacement of 0.117 in. occurs not on the panel itself but at the ends of the upper repair pieces at their sections which overwrap the pultruded rod and above the machined slots, which makes them not directly attached to the web and, consequently, springing upwards. The maximum out-of-plane displacement for the repaired panel itself occurs in the direct vicinity of the simulated damage, marked as point B in Figure 18, and is even smaller, i.e. 0.105 in. Furthermore, if the location resulting in the maximum out-of-plane displacement for the pristine panel, point A in Figure 17, is examined for the repaired panel, point C in Figure 18, it shows the out-of-plane displacement of 0.043 in., which differs from the pristine panel only by 0.009 in.

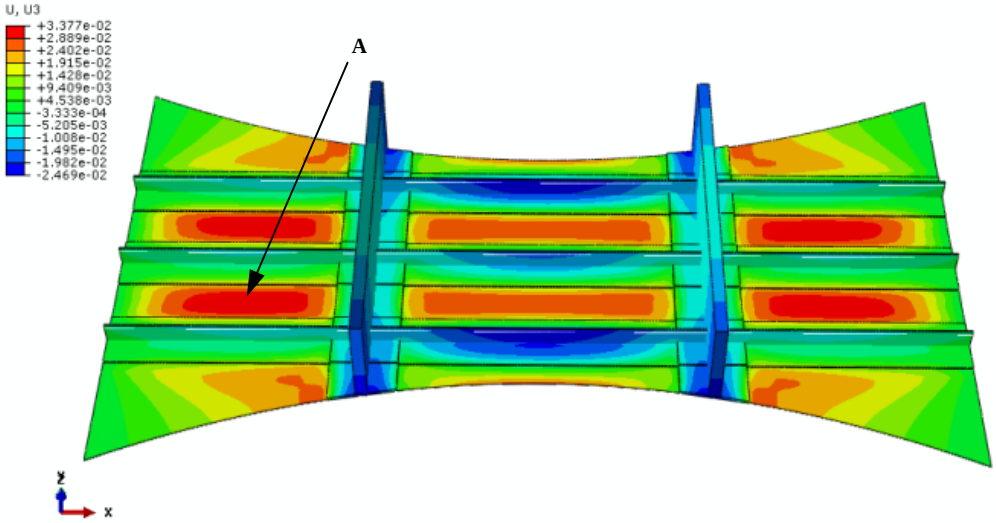

Figure 17. Pristine panel out-of-plane displacement, in.

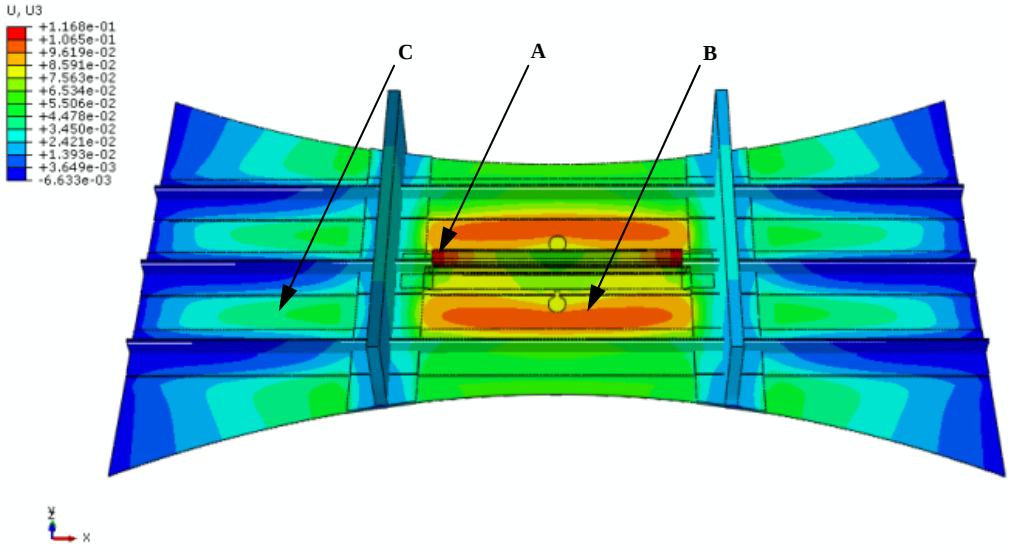

Figure 18. Repaired panel out-of-plane displacement, in.

The maximum principal strain distribution for the pristine panel on its substructure side is presented in Figure 19. The same maximum principal strain distribution for the repaired panel, with the repair assembly pieces not shown, is presented in Figure 20. Note that in both figures the strain levels coded with the red color extend to

the assumed ultimate tension load strain allowable of 0.0105 in./in., i.e. 1.5 times 0.0070 in./in., considered in this work as the limit tension load strain allowable. The grey-coded areas, therefore, designate regions where the ultimate allowable strain is exceeded according to the analysis. These regions, however, occur primarily in the vicinity of the panel cross-section discontinuities around the frame caps. In these regions the flanges comprising of three stacks transition to frame cap sections which comprise of six stacks, and the single-stack skin transitions to frame cap sections which comprise of four stacks, as shown in Table 4. Consequently, the high levels of maximum principal strain are assumed to be due to discontinuities. Analysis of these localized effects is not in the scope of the present work. Local analyses using StressCheck® software and testing, both conducted by The Boeing Company, confirmed in the past that these areas at the load levels considered herein are not exceeding material allowables. Also note, that high strain levels in the regions where the pultruded rod is phased-out in the repaired configuration, designated in Figure 20 as region A, are also considered to be overestimated because the pultruded rod of up to 0.375-in. diameter is modeled with 1-D beam elements which share only one row of nodes with the web shell elements. Consequently, rod and its overwraps are not accurately modeled and the load transition between these elements is not accurately evaluated in this study. The interactions between these elements is being evaluated elsewhere in the PRSEUS program.

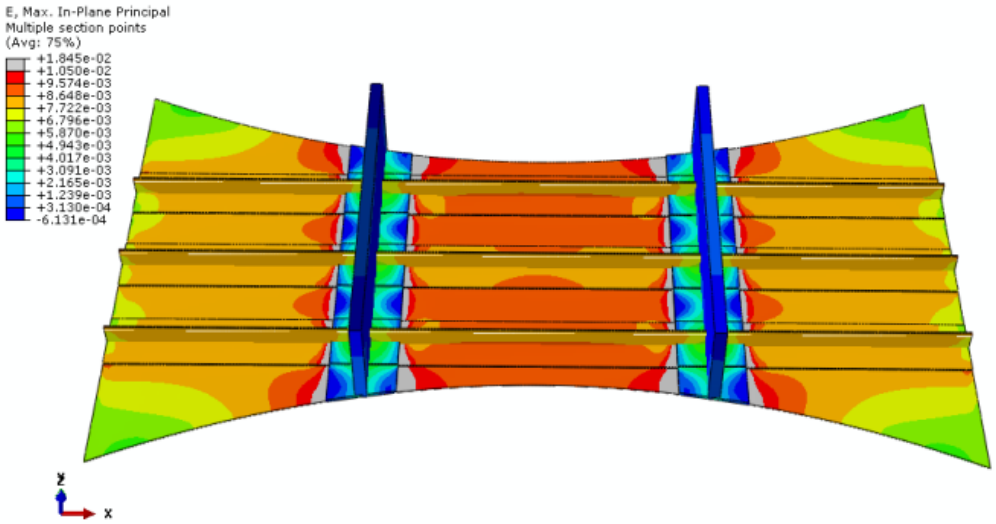

Figure 19. Pristine panel maximum principal strain, in./in.

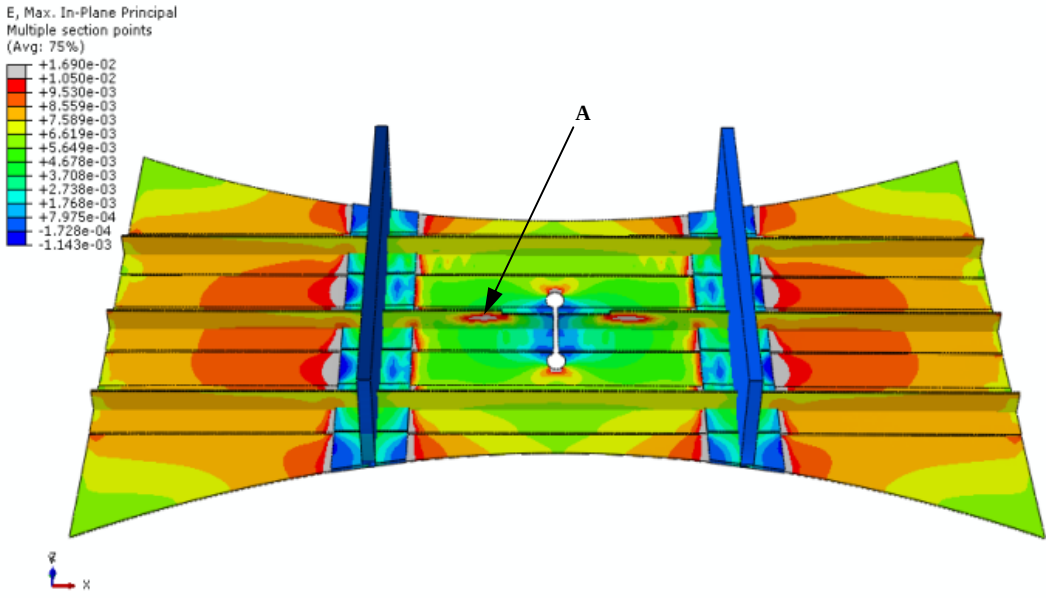

Figure 20. Repaired panel maximum principal strain with the repair assembly removed, in./in.

The maximum principal stress distributions for the aluminum alloy repair assembly pieces are presented in Figure 21 for the upper Mohawk piece and in Figure 22 for the lower strap. Similar to the strain results presented above for the composite parts, the red color code extends to the ultimate tension load stress allowable of 78 ksi. The only small areas where these values obtained from the FE analysis are exceeded are located at the tips of the machined slots of the upper Mohawk repair assembly, location A in Figure 21. The stress levels at these locations are likely overestimated due to discontinuities. Additionally, small areas where the maximum principal stresses exceed the elastic yielding stress of 69 ksi (apart from the already mentioned region A in Figure 21) occur at the mid-span locations of the repair pieces in the vicinity of the simulated saw-cut damage and are designated as location B in Figure 21 and location A in Figure 22. Note, that the Mohawk repair assembly parts were verified not to exceed the yielding stress at the limit load of 146 kip.

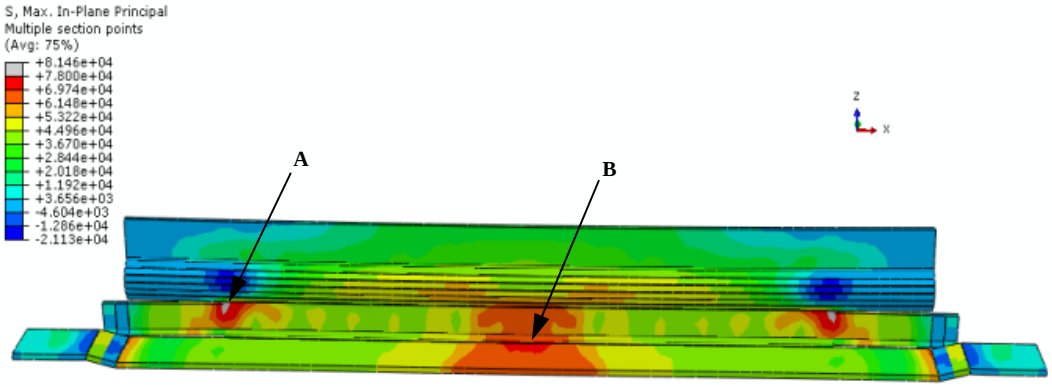

Figure 21. Upper repair maximum principal stress, ksi.

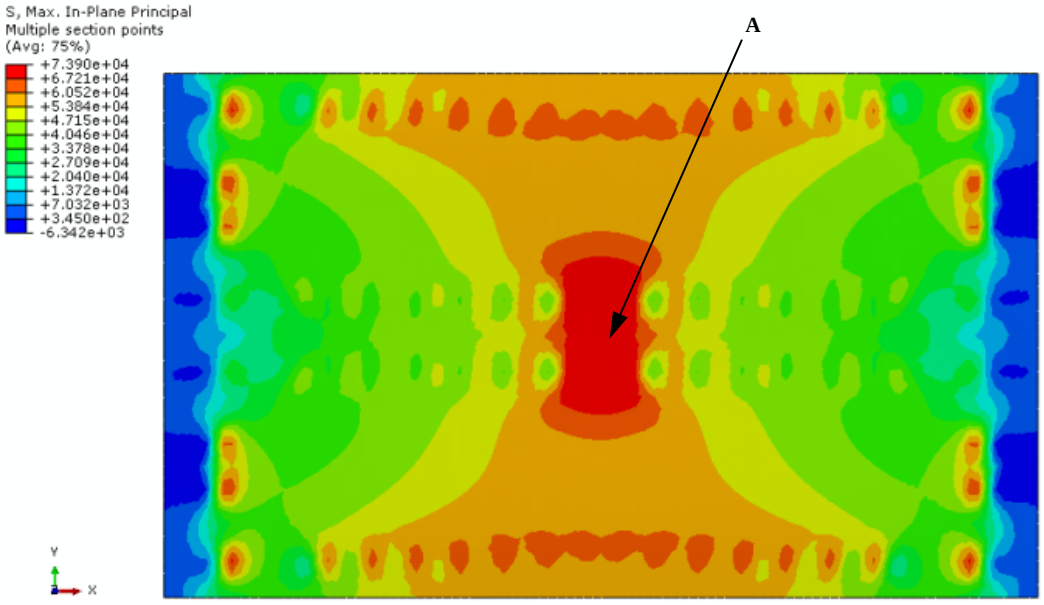

Figure 22. Lower strap maximum principal stress, ksi.

Once the assessment of the strain and stress results of the general sections of the composite panel and the metallic Mohawk repair parts was accomplished, the bearing stress-bypass strain analysis in the vicinity of fastener attachments of the repair assembly to the damaged panel was performed. Bearing stress and bypass strain levels turned out to be a limiting factor in the Mohawk repair design, particularly in the area of the upper repair assembly attachment to the stringer's web. This location was previously identified as critical for the single-stringer panel repair design. Similarities between the single-stringer panel repair and the present design included the limited distance between the flange and the pultruded rod reducing the diameter of fasteners that can be applied in this region to 0.19 in. (i.e. smaller than the 0.25 in. used on the panel's horizontal surfaces), the very thin stringer's web

(0.104 in.), and the proximity of the pultruded rod which is the most stiff component of the panel. The bearing stress and bypass strain results of this most critical fastener attachment are presented next, although all the attachments were investigated in the fashion described below.

The results obtained for the upper repair assembly attachment to the stringer's web are illustrated in Figure 23 where two curves represent the distribution of the bearing stress and bypass strain from the frame (0 in.) to the panel mid-length location (10 in.). The repair is symmetric so the results for only half of the repaired section are shown. Bearing stress is shown as a red line and bypass strain is shown as a blue line. Each data point represents one fastener location. It is seen that the bearing stress values peak at the two locations corresponding to the end fasteners presented in the plot. A high value of the bearing stress is also found at the location corresponding to a fastener located closest to the end of the machined slot in the upper Mohawk repair piece. The remaining fasteners transfer significantly lower loads from the panel to the upper repair assembly. While the ideal bearing stress values would approach constant distribution with maximum values less than the allowable levels, a more illuminating discussion can be held by comparing the bearing stresses obtained from the best design arrived to thus far with the one considered earlier in the effort, which was not optimized. Since only one, best solution was being presented in the paper thus far, for the purpose of the subsequent discussion regarding Figure 24, this solution is referenced as 'improved' and the one considered earlier is referenced as 'baseline.' The bearing stress distributions based on the baseline and the improved designs are presented in Figure 24 where the baseline is shown in black and the improved design, repeated from Figure 23, is shown in red. The baseline design did not have the machined slots in the upper repair assembly and the pultruded rod taper in the vicinity of the simulated saw-cut damage was not introduced. Without the machined slots in the upper repair pieces, the fourth fastener from the left is seen to carry much lower load, and the overall bearing stress distribution is characterized by one extensive valley-like shape, rather than two smaller drops. The improvement of the design closer to the simulated saw-cut damage (data points on the right end of the two curves) is also attributable to a more efficient design of the pultruded rod termination. Consequently, the total load that is transferred from the damaged stringer to the upper Mohawk repair assembly is maintained while the peak bearing stress values are decreased. In order to further diminish the differences in the bearing stress level distribution, a continuously varying repair piece cross-section along the span of the repair assembly, or otherwise significantly more complex repair geometry, would be required. Finally, the bypass strain for the improved configuration, presented in Figure 23, has also a fluctuating distribution but excluding the two far right data points the fluctuations are not large. As expected, the most significant drop occurs close to the saw-cut damage since the center stringer needs to be completely unloaded before it is terminated.

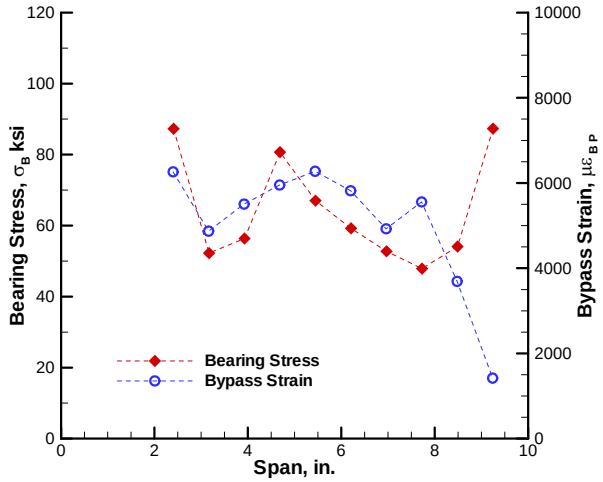

Figure 23. Distribution of the bypass strain and the bearing stress along at the center web.

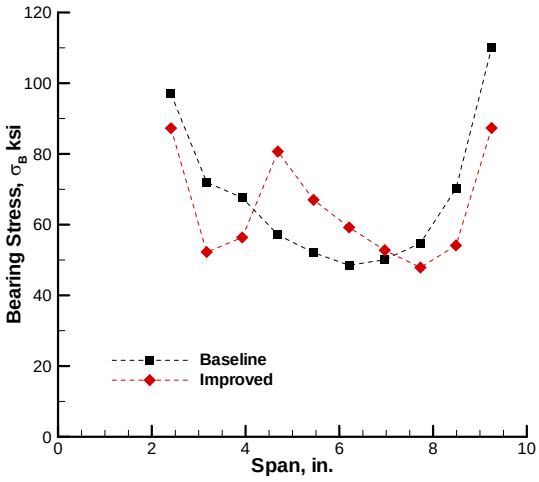

Figure 24. Bearing stress comparison between baseline and improved designs.

Figure 25 presents the results from Figure 23 in the format of Figure 14. While the spatial distribution information is lost, this representation of the results enables assessment of the structural integrity of the design based on test data allowables illustrated in Figure 14. Allowable values representative of the dashed blue and green trend lines from Figure 14 are not plotted in Figure 25 since these values are proprietary. Note, that the points in Figure 25 form a pattern highlighted by a green dashed line with its limits established by the two end fastener locations near the frame and the saw-cut.

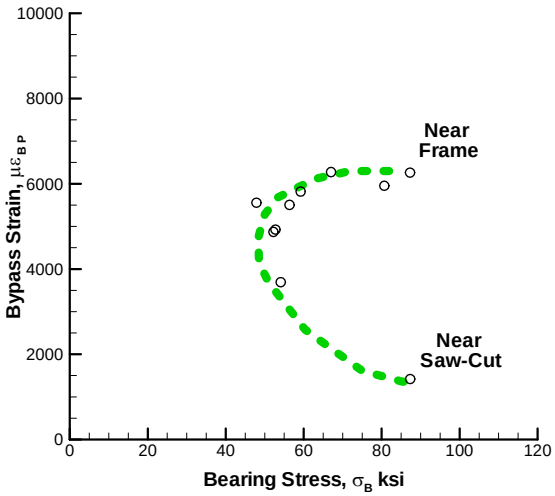

Figure 25. Bearing stress-bypass strain analysis at the center web.

VII. Design assessment

The fastener-based attachments of the metallic repair assembly to the composite panel have a major impact on the repair design. For the case studied, particularly the attachment of the upper Mohawk assembly to a thin stringer's web in the proximity of a stiff pultruded rod represents a critical location as its design envelope was found to be limited by multiple factors. In the proposed design, the maximum number of fasteners complying with their spacing guidelines is accommodated in the available span of the web. Furthermore, additional enhancements such as machined slots tailoring the compliance of the upper repair assembly and a gradual phase-out of the pultruded rod are incorporated in the design. The bearing stress levels cannot be further reduced by designing a more compliant metallic repair assembly because it is already approaching its ultimate load carrying capability. While designing a continuously variable cross-section repair assembly could have some benefits, it has limited practical application because the repair would need to be "one of the kind" and more complicated to manufacture. It would also be difficult to maintain the neutral bending axis of the original structure into the repair. Therefore, the design of the metallic repair assembly pieces is deemed to represent a reasonable compromise. On one hand, the repair parts are not complicated from the manufacturing point of view and can be customized to make them applicable to a range of possible damage forms, as demonstrated before with the single-stringer panel test. On the other hand, their load carrying capability is well utilized as evidenced by an onset of the plastic response regime as the ultimate load levels are approached. Consequently, the weight penalty associated with the designed repair is also limited.

Further work is warranted in the area of the PRSEUS panel metallic repair design and analysis. Note that the damage investigated in the present effort is centrally located between frames. If a similar damage was located away from the mid-bay location, a shorter distance from the frame to the damaged location would reduce the number of installed fasteners and further increase the bearing stress levels, potentially to a point when extending the repair onto the next bay would be necessary. Extending the repair assembly beyond the bay that contains the damage (i.e. beyond the two consecutive frames) would involve additional complications arising from a need to introduce frame cut-outs. Also note that composite material allowables in compression are typically lower than the material allowables in tension. Consequently, a repair that is feasible under tension loading may be insufficient under a similar level of compression loading.

VIII. Concluding Remarks

The feasibility of applying a metallic repair to a panel fabricated using the PRSEUS concept and containing severe but localized damage was considered. The study involved design, analysis and basic optimization of a repair applicable to PRSEUS structures. Results from a FE analysis approach were compared to available test data. Once confidence in the modeling approach was established it was used as a primary tool in the design and optimization efforts. Baseline requirements for the load carrying capability of the repaired structure were derived from the pristine panel analysis and available test results. Several repair configurations were analyzed and assessed. The most structurally efficient manufacturable configuration was presented and its limiting features identified.

Advanced FE modeling techniques, such as use of compliant fasteners defined using connector elements and their node-independent placement in the model that can be easily modified without need for mesh modifications, were utilized in the study. Geometrically nonlinear analysis runs were conducted and the metallic repair assembly accounted for a nonlinear elastic-plastic material behavior. The fidelity of the analysis streamlined exploration of multiple design variations aimed at arriving at an efficient repair configuration. A tension test of a repaired panel is being planned to validate analysis tools and refine them as necessary.

Acknowledgments

The author wishes to thank Dawn Jegley and Andrew Lovejoy of NASA Langley Research Center, Structural Mechanics and Concepts Branch, Hampton, VA and Alex Velicki and Kim Linton of The Boeing Company, Boeing Research and Technology, Huntington Beach, CA for their helpful discussions during the course of this work. The author also gratefully acknowledges the test data and other test documentation received from The Boeing Company, Advanced Structures Research and Development, which facilitated these studies and helped in preparation of this manuscript.

References

[1]Li, V. and Velicki, A., "Advanced PRSEUS Structural Concept Design and Optimization," *Proceedings of the 12th AIAA/ISSMO Multidisciplinary Analysis and Optimization Conference*, AIAA-2008-5840, Victoria, BC, Canada, 2008.

[2]Jegley, D. C., Velicki, A., and Hansen, D. A., "Structural Efficiency of Stitched Rod-Stiffened Composite Panels with Stiffener Crippling," *Proceedings of the 49th AIAA/ASME/ASCE/AHS/ASC Structures, Structural Dynamics and Materials Conference*, AIAA-2008-2170, Schaumburg, IL, 2008.

[3]Velicki, A., Thrash, P., and Jegley, D. C., "Airframe Development for the Hybrid Wing Body Aircraft," *Proceedings of the 47th AIAA Aerospace Sciences Meeting Including The New Horizons Forum and Aerospace Exposition*, AIAA-2009-932, Orlando, FL, 2009.

[4]Yovanof, N. P., Velicki A., and Li, V., "Advanced Structural Stability Analysis of a Nonlinear BWB-Shaped Vehicle," *Proceedings of the 50th AIAA/ASME/ASCE/AHS/ASC Structures, Structural Dynamics and Materials Conference*, AIAA-2009-2452, Palm Springs, CA, 2009.

[5]Velicki, A. and Thrash, P., "Advanced Structural Concept Development Using Stitched Composites," *Proceedings of the 49th AIAA/ASME/ASCE/AHS/ASC Structures, Structural Dynamics and Materials Conference*, AIAA-2008-2329, Schaumburg, IL, 2008.

[6]Velicki, A., "Damage Arresting Composites for Shaped Vehicles, Phase I Final Report," NASA CR-2009-215932, NASA Langley Research Center, Hampton, VA, September 2009.

[7]Composite Aircraft Structure, Advisory Circular AC No. 20-107B, U.S. Department of Transportation, Federal Aviation Administration, August 2010.

[8]ABAQUS version 6.10-1 On-line Documentation, ABAQUS Analysis User's Manual, Dassault Systemes Simulia Corp., Providence, RI, 2010.

[9]Title 14 Code of Federal Regulation, Part 25 "Airworthiness Standards: Transport Category Airplanes," Subpart C "Structure," §25.305, Electronic Code of Federal Regulations, http://ecfr.gpoaccess.gov

[10]Karal, M., "AST Composite Wing Program – Executive Summary," NASA CR-2001-210650, NASA Langley Research Center, Hampton, VA, March 2001.

[11]Velicki, A., Yovanof, N., Baraja, J., Linton, K., Li, V., Hawley, A., Thrash, P., DeCoux, S., and Pickell, R., "Damage Arresting Composites for Shaped Vehicles – Phase II Final Report," NASA CR-2011-216880, NASA Langley Research Center, Hampton, VA, January 2011.

[12]MSC.Nastran 2005 r2 Release Guide, MSC Software Corporation, Santa Ana, CA, 2005.

[13]Mirsamadi, S., "Advanced Subsonic Technology (AST) Composite Wing Material Stiffness and Allowable Strength Properties for Stitched Composite Laminates," Report Number 98K0318 (proprietary), The Boeing Company, Advanced Transport Aircraft Development, Long Beach, CA, September 1998.

[14]Neal, B. and Herr, A., "Pin Bearing and Bearing Bypass Testing, Damage Arresting Composites," test report (proprietary), The Boeing Company, Research and Technology, St. Louis, MO, March 2009.